Article

NMR Spectra Particularities in LiNbO$_3$ Crystals with a Near-Stoichiometric Composition

Alexander Yatsenko [1] , Sergey Yevdokimov [1], Mikhail Palatnikov [2,*] and Nikolay Sidorov [2]

[1] Institute of Physics and Technology (Structural Subdivision), V.I. Vernadsky Crimean Federal University, Vernadsky Av. 4., 295007 Simferopol, Republic of Crimea, Russia
[2] Tananaev Institute of Chemistry—Subdivision of the Federal Research Centre «Kola Science Centre of the Russian Academy of Sciences», 184209 Apatity, Russia
* Correspondence: m.palatnikov@ksc.ru

Abstract: The paper studies LiNbO$_3$ (LN) crystals with a near-stoichiometric composition (NSLN). The study establishes the possibility of different physical methods to reveal NSLN crystals' exact composition. The main goal was to establish how precisely these methods can reveal a NSLN composition, including a defective structure. This structure determines properties that are important for the application of the crystals. Two NSLN crystals with a different Li/Nb ratio have been studied by IR and NMR spectroscopy. NSLN crystals have been grown from a congruent melt with different K$_2$O flux contents (5.0 and 5.5 wt%). The data on NSLN have been compared with the data on congruent (CLN) crystals. CLN are the most widely used LN crystals. The study has established that analysis of the IR spectra can determine the Li/Nb ratio within [Li$_2$O] = 48.6 – 50.0 mol% range, while the ^{93}Nb NMR spectra has a wider range of sensibility. LN crystals' stoichiometry or the Li/Nb ratio determine the concentration of antisite defects Nb$_{Li}$. Niobium substitutes lithium in its octahedron. Such defects appear up to [Li$_2$O] = 49.9 mol%. Thus, the study shows that IR and NMR spectroscopy are sensitive methods that can complement each other when determining the precise LN composition (Li/Nb ratio) and the presence of intrinsic defects in the crystals.

Keywords: lithium niobate; stoichiometry; NMR spectroscopy; IR spectroscopy

1. Introduction

LiNbO$_3$ (NL) lithium niobate crystals are one of the most demanded ferroelectric materials at the present time [1–5].

Particular attention is paid to crystals with a composition close to stoichiometric (near stoichiometric lithium niobate, NSLN). Their most pronounced features are their increased resistance to optical damage, a significantly lower value of the coercive field [1], and relatively low absorption up to the far IR region [6]. These particularities of the LN crystal determine its wide application in different optical devices. At this, NSLN crystals' properties and their defective structure strongly depend on the slightest changes in the Li/Nb ratio [6–9]. However, modern literature fails to provide enough information of such studies. Therefore, it is important to know the exact concentration range in which various physical methods can be applied with enough accuracy. The methods determine the composition and thus, the defective structure of NSLN.

LN is a phase of variable composition; its homogeneity range is quite wide. In this case, the composition of congruent melting is such a nonstoichiometric composition ([Li$_2$O] = 48.6 mol%), in which the composition of the melt strictly corresponds to the composition of the grown crystal. The phase diagram of a Li$_2$O-Nb$_2$O$_5$ system is widely discussed, as shown in Figure 1.
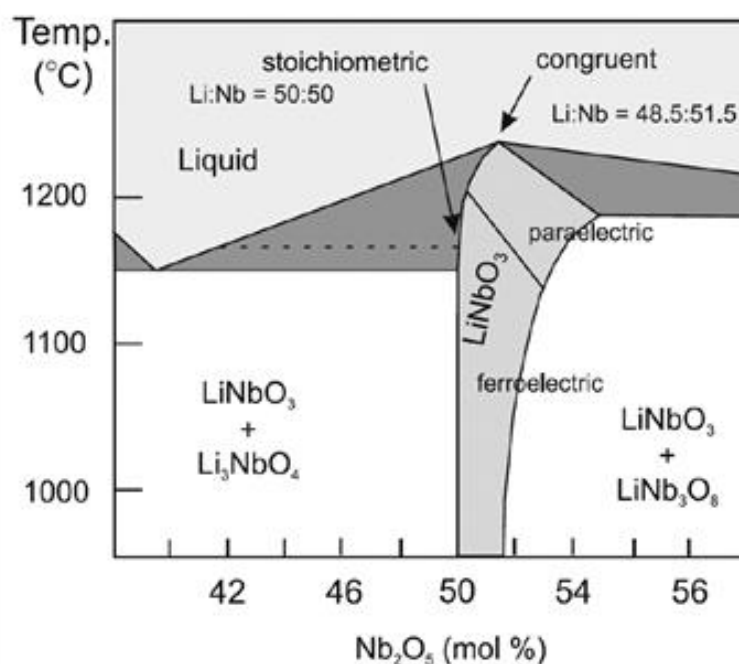
Figure 1. Phase diagram of a binary system Li_2O-Nb_2O_5. Reprinted with permission from Ref. [1], 2008, Springer.

The nonstoichiometric nature of a congruent lithium niobate (CLN) crystal predetermines the developed defect structure and specific defects. The defects are associated with the antisite arrangement of intrinsic cations in the crystal lattice: Nb_{Li} — niobium occupies the lithium site of an ideal structure. Vacancies appear in the lithium sublattice (Li_V) for charge compensation. Despite such a large number of antisite defects, the CLN crystal has a high compositional and optical uniformity.

Near-stoichiometric lithium niobate (NSLN) crystals studied in this work (NSLN1 and NSLN2) were grown from a congruent melt containing an excess of the alkali component K_2O, 5 and 5.5 wt% correspondingly. Growing such crystals is a typical solution-melt process or top seeded solution growth. The K_2O solution is unique, it provides the possibility to grow large almost stoichiometric NSLN crystals; optical uniformity of such crystals is high, though it is slightly less than the uniformity of CLN crystals. Potassium does not incorporate into the crystal structure. A comparison of Li^+ and K^+ ionic radii (0.68 Å and 1.38 Å, respectively) proves that incorporation is impossible. The melt composition for growing NSLN crystals with K_2O flux changes much less than the melt composition during the growth of pure stoichiometric (SLN) crystals from a melt with excess lithium ($[Li_2O] \approx 58.6$ mol%). Thus, optical and compositional uniformity increases in the row SLN, NSLN, CLN.

The nuclear magnetic resonance (NMR) applied to nuclei with their own quadrupole moment is very sensitive to local distortions of the structure of the LN crystal [7]. Three types of quadrupole nuclei, [6]Li, [7]Li, and [93]Nb, are present in the LN crystals. This feature predetermined the wide application of the NMR method for studying this material.

An early stage of study of NL crystals shows that the composition of the initial mixture (meaning R = Li/Nb) strongly affects the shape of the line of the central transition of the [93]Nb NMR spectrum in polycrystalline ceramic samples [8,9]. At that time, the problem of synthesizing LN single crystals with a composition really close to that of stoichiometric had not been solved yet. Therefore, it is impossible to unambiguously evaluate the results presented in work [9].

^{7}Li NMR in NSLN crystals grown by the Czochralski method from a melt with an excess of Li_2O was studied in [10]. It was shown that the dependence of quadrupole coupling constants $C_z(T)$ is a linear function of temperature, and at room temperature the

values of C_z for all samples coincide within the error. Additional information on the effect of nonstoichiometry of crystals on the NMR spectrum parameters at room temperature is absent from [10].

Information on ^{93}Nb NMR studies in NSLN samples is scarce. The results of studying the dependence of the line width $\delta\nu$ of the central transition of the ^{93}Nb NMR spectrum on the angle θ between the direction $\mathbf{B}_o$ and the polar axis of the crystal Z in a series of LN crystals of different compositions, including the NSLN sample, are presented only in [11]. The NSLN sample was grown under K_2O flux. It was stated in [11] that the line width does not depend on the angle θ between the polar axis of the crystal and the direction of the magnetic field $\mathbf{B}_o$, but neither the conditions for the experiment nor the method used to detect ^{93}Nb NMR were specified. Moreover, the dependences $\delta\nu(\theta)$ of congruent (CLN) and a magnesium-doped LN presented in [11] do not coincide with other known data either qualitatively or quantitatively [12–14].

The most characteristic features of the NMR spectra of CLN crystals are the presence of additional weak side lines in the ^{7}Li spectra and the presence of a weak additional line of the central transition in the ^{93}Nb spectrum. A weak additional line of the central transition of the ^{93}Nb spectrum corresponds to the nuclei of antisite Nb_{Li} cations [12,13,15]. In addition, a significant broadening of the lines in the ^{93}Nb NMR spectrum is observed in comparison with the natural width in CLN. The natural width is determined only by direct magnetic dipole—dipole interactions.

The goal of this study is to evaluate the concentration range of applicability of NMR and IR spectroscopy methods for researching the stoichiometry and structural perfection of NSLN crystals, and to test the validity of some hypotheses that have been put forward in the literature to explain the complex structure of the ^{7}Li and ^{93}Nb NMR spectra. In addition, the study presents a comparative analysis of various methods of mathematical processing of the line contours of the IR spectrum of NL crystals. The analysis will help to find out the most accurate way to determine the stoichiometry of LN crystals of various compositions.

2. Materials and Methods

The experiments were performed on two near-stoichiometric $LiNbO_3$ crystals (NSLN) grown with the addition of 5.0 and 5.5 wt% K_2O to the melt (NSLN1 and NSLN2, respectively). These crystals were grown in the Tananaev Institute of Chemistry. The crystals were grown at a low growth rate (0.25 mm/h); post-growth annealing of the crystal boule was carried out at 1200 °C for 20 h. Single crystals were turned to a single domain state by high-temperature electro-diffusion annealing by cooling the samples at a rate of 20 K/h in the temperature range (1220–890) °C under an external electric field [16].

NSLN1 and NSLN2 crystals were grown by HTTSSG (High temperature top seed solution growth) from a melt with a K_2O flux. Crystals were grown with a free access of the atmospheric air from platinum crucibles 75 mm in diameter. Axis grade was relatively low, 2–4 deg/cm. LN crystals were grown along the polar axis Z. Rotation speed was 13–15 rpm. These exactly crystals were grown on the Granat equipment (ELS/Elan, Moscow, Russia), Figure 2a. The installation is equipped with an automatic crystal diameter control system (ELS, Moscow, Russia). The thermal unit design creates an isothermal zone in the volume of the platinum screen for post-growth annealing of crystals; NSLN crystals grow at a relatively small temperature gradient at the crystallization front. The grown NSLN1 and NSLN2 crystals had a flat crystallization front and close geometric sizes: diameter d ≈ 30–33 mm, the length of the cylindrical part L_c ≈ 30–36 mm. Figure 2b shows NSLN crystals grown from a melt with the addition of 5.0 and 5.5 wt% K_2O.

(**a**)

(**b**)

Figure 2. Granat facility for growing LN crystals by the Czochralski method (**a**); NSLN1 and NSLN2 crystals after disassembling the thermal unit (**b**). Figure 2a is reprinted with permission from Ref. [17], 2022, Elsevier.

The LN charge was synthesized by solid-phase synthesis. Lithium carbonate Li_2CO_3 (not more than 3×10^{-4} wt% impurities, Sigma Tek, Khimki, Russia) and niobium pentoxide Nb_2O_5 (99.9, Solikamsk magnezium works, Solikamsk, Russia) were mixed in in the "drunken barrel". After that the mixture was sintered. A granular charge of the congruent composition ($[Li_2O]$ = 48.6 mol%) was obtained from these initial components by the method of synthesis-granulation. The charge had a high bulk density of about 3.4 g/cm^3. The composition of impurities of the LN charge and NSLN1 and NSLN2 crystals was determined by spectral analysis. The composition is provided in Table 1.

Table 1. Impurity composition of the initial charge and two studied NSLN crystals.

Impurity	Impurity Concentration, wt%		
	In the Charge	In NSLN1	In NSLN2
Mn, V, Mg, Sn, Cu	$<2 \times 10^{-4}$	$<3 \times 10^{-4}$	$<4 \times 10^{-4}$
Pb, Ni, Cr	$<2 \times 10^{-4}$	$<3 \times 10^{-4}$	$<2 \times 10^{-4}$
Co, Mo	$<3 \times 10^{-4}$	$<4 \times 10^{-4}$	$<3 \times 10^{-4}$
Si, Fe	$<3 \times 10^{-4}$	$<3 \times 10^{-4}$	$<3 \times 10^{-4}$
Ti	$<3 \times 10^{-4}$	$<4 \times 10^{-4}$	$<5 \times 10^{-4}$
Al	$<8 \times 10^{-4}$	$<7 \times 10^{-4}$	$<6 \times 10^{-4}$
Zr	$<5 \times 10^{-4}$	$<6 \times 10^{-4}$	$<7 \times 10^{-4}$
Ca	$<4 \times 10^{-4}$	$<6 \times 10^{-4}$	$<5 \times 10^{-4}$
Te, Sb	$<4 \times 10^{-4}$	$<5 \times 10^{-4}$	$<4 \times 10^{-4}$
Bi	$<3 \times 10^{-4}$	$<4 \times 10^{-4}$	$<4 \times 10^{-4}$

XRD patterns of crystals were registered by the diffractometer DRON-6 (NPP Burevestnik, Sankt-Peterburg, Russia) in a monochromatic CuKα radiation (tube voltage 35 kV, current 20 mA) in scattering 2θ angles, at a range of 2–115°. The stability of the recording circuit was monitored during measurements. Moreover, the XRD pattern was recorded several times for each studied sample. The accuracy in determining the intensity at each point of the diffraction line was no less than 5%. The XRD patterns of all nominally pure LN crystals under study (NSLN1, NSLN2, CLN1, CLN2, and CLN3) are qualitatively similar and correspond to the XRD pattern of LN with space symmetry group R3c. There is only a slight (within the measurement error) mutual redistribution of intensities for reflections (204) and (116), Figure 3.

Structure characteristics and the defective structure of NSLN and CLN crystals are studied in detail in the works [17,18].

The CLN crystals were synthesized by the Czochralski method in NPO Karat (Lviv, Ukraine) and the Tananaev Institute of Chemistry. IR studies were carried out on two nominally pure congruent LN crystals, CLN1 and CLN2. The sample CLN1 was thermochemically treated in a wet air atmosphere at a temperature of 1073 K for 8 h. Due to the high content of water vapor in the atmosphere, such treatment noticeably increases the volume concentration of hydrogen in the crystal. The third crystal of this row, CLN3, was used for the NMR experiment.

Table 2 shows some characteristics of these samples, including the expected content of Li_2O and the relative amount of Nb_{Li} antisite ions: $N' = n(Nb_{Li})/n(Nb_{Nb})$. Parameters given in Table 2 were determined according to the calculations in [19] (column A) and [20] (column B). References [19,20] present two experimentally obtained dependences of the composition of the crystal on the content of K_2O in the charge during the growth of NSLN crystals with K_2O flux. The dependences were used to evaluate NSLN 1 and NSLN 2 crystals compositions.

Table 2. Characteristics of LN crystal samples used in the experiment.

Sample	K_2O in charge, wt%	Li_2O mol%		N', %	
		A	B	A	B
CLN3	-	48.6	48.6	1.08	1.08
NSLN1	5.0	49.55	49.66	0.298	0.216
NSLN2	5.5	49.7	49.77	0.199	0.153

The study of IR absorption spectra in the range of OH-group stretching vibrations in the range of 3400–3600 cm^{-1} was performed on an FTIR spectrometer FSM-2202 (Infraspek, Russia, Saint-Petersburg) with a resolution of 0.5 cm^{-1}. The measurements were performed on z-cut samples under unpolarized radiation and at room temperature.
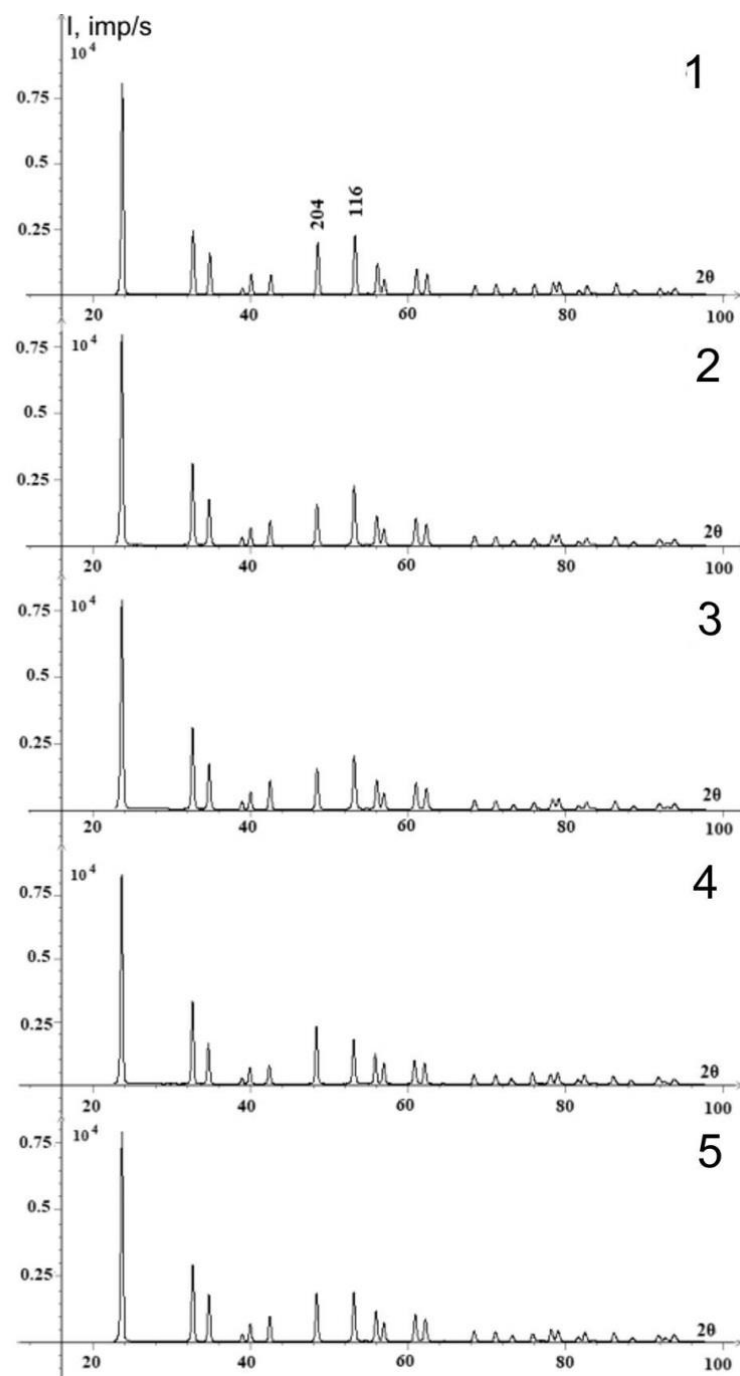
Figure 3. XRD patterns of powdered samples of NSLN1 (**1**); NSLN2 (**2**); CLN1 (**3**); CLN2 (**4**); and CLN3 (**5**).

NMR spectra were recorded on a continuous wave wide-line spectrometer with an autodyne detector developed by authors [21] under sweep and modulation of a magnetic field and fixed resonant frequency. All experiments were carried out in a magnetic field; $B_o \sim 1.2$ T for ^{7}Li nuclei and $B_o \sim 1.4$ T for ^{93}Nb nuclei using the multiple accumulation technique.

3. Results and Discussion

3.1. Analysis of Composition of Real LN Crystals by Means of IR Spectroscopy

The stoichiometry of nominally impurity-free LN crystals strongly influences the IR absorption spectrum in the region of OH groups stretching vibrations [22]. This region of spectrum can contain at least three bands, their position corresponds to wave numbers

$\overline{v_1}$ = 3468 cm^{-1}, $\overline{v_2}$ = 3482 cm^{-1}, and $\overline{v_3}$ = 3492 cm^{-1} [22]. The presence of these bands is confirmed by other investigators [23,24]. More than that, the example of the isostructural LiTaO$_3$ crystal reveals that $\overline{v_1}$, $\overline{v_2}$, $\overline{v_3}$ linearly depends on the R value [25].

Several ways to determine the real composition (R = Li/Nb) of nominally pure LN crystals by analyzing IR spectra were reported [6,23,26]. These methods require the decomposition of spectra and determination of integral intensity of each band. When decomposed, the individual shape of the bands is represented either by the Lorentz distribution [6,23,25], the Gaussian distribution [26], the product of the Lorentz and Gauss distributions [27], or the so-called Voigt pseudo distribution (pseudo-Voight, PV) [28]. PV is a linear combination of the Lorentz $L(\overline{v})$ and Gauss $G(\overline{v})$ distributions:

$$PV(\overline{v}) = \eta L(\overline{v}) + (1 - \eta)G(\overline{v})$$

where the parameter η varies in the range between 0 and 1, and FWHM (full width at half maximum) can be different for $L(\overline{v})$ and $G(\overline{v})$ distributions. The application of PV is caused by the presence of both uniform (Lorentz distribution) and non-uniform (Gauss distribution) widening. According to the moments, for the Gaussian line, $M_2 = \Delta^2$, and the line width between the maxima is $\delta v = 2\Delta$.

We evaluated the degree of stoichiometry of studied samples due to a method in [6]. We analyzed the IR spectra of two congruent LN samples with different hydrogen content, CLN1 and CLN2. We calculated R due to a method from [23].

Real composition of NSLN crystals due to [6] can be determined by a ratio between integral intensities of IR bands corresponding to wave numbers $\overline{v_1}$ = 3466 cm^{-1}, $\overline{v_2}$ = 3480 cm^{-1}, I_1 and I_2.

$$M = 50 - \frac{1}{1.933} \cdot \frac{I_1}{I_2} \text{ (mol\%)} \tag{1}$$

where *M*—content of Li$_2$O in sample in mol%. Thus, R = $M/(1 - M)$.

Three main lines were assumed in the IR absorption spectra simulation, their wave numbers are close to the specified $\overline{v_1}$, $\overline{v_2}$, $\overline{v_3}$ values. Several options for the individual shape of the spectrum components were considered:

(a)   Each spectral band was represented by the Lorentz distribution (L-L-L);
(b) $\overline{v_1}$ = 3466 cm^{-1} and $\overline{v_3}$ = 3490 cm^{-1} bands were represented by the Lorentz distribution; $\overline{v_2}$ = 3480 cm^{-1} band was represented by the Gaussian distribution (L-G-L);
(c)   All bands were represented by Voigt pseudo distribution (PV-PV-PV).

Approximation accuracy was determined by the following criterion $\Delta\alpha(\overline{v}) = \alpha_{exp}(\overline{v}) - \alpha_{calc}(v)$ difference function minimization due to the equation

$$\mu = \frac{\sum_{i-1}^{k} |\Delta\alpha_i|}{\sum_{i-1}^{k} (\alpha_i)_{exp}} \tag{2}$$

where $(\alpha_i)_{exp}$ is experimental, $(\alpha_i)_{calc}$ is the calculated value of the coefficient of optical absorption at the i-th point of the spectrum in the area from 3405 to 3550 cm^{-1}.

Figures 4–7 demonstrate the IR spectra of the studied samples and the results of their optimal decomposition corresponding to the minimum value of μ. Figures 4–7 also present corresponding $\Delta(\alpha)$ functions. IR absorption spectra modeling taking into account only three main spectral components leads to a quite satisfactory correspondence of the simulated spectra to the real ones, and the $\Delta\alpha(\overline{v})$ value is comparable to the noise components (excluding NSLN2 sample) and no more than 3% of the maximum of $\Delta\alpha$ value.
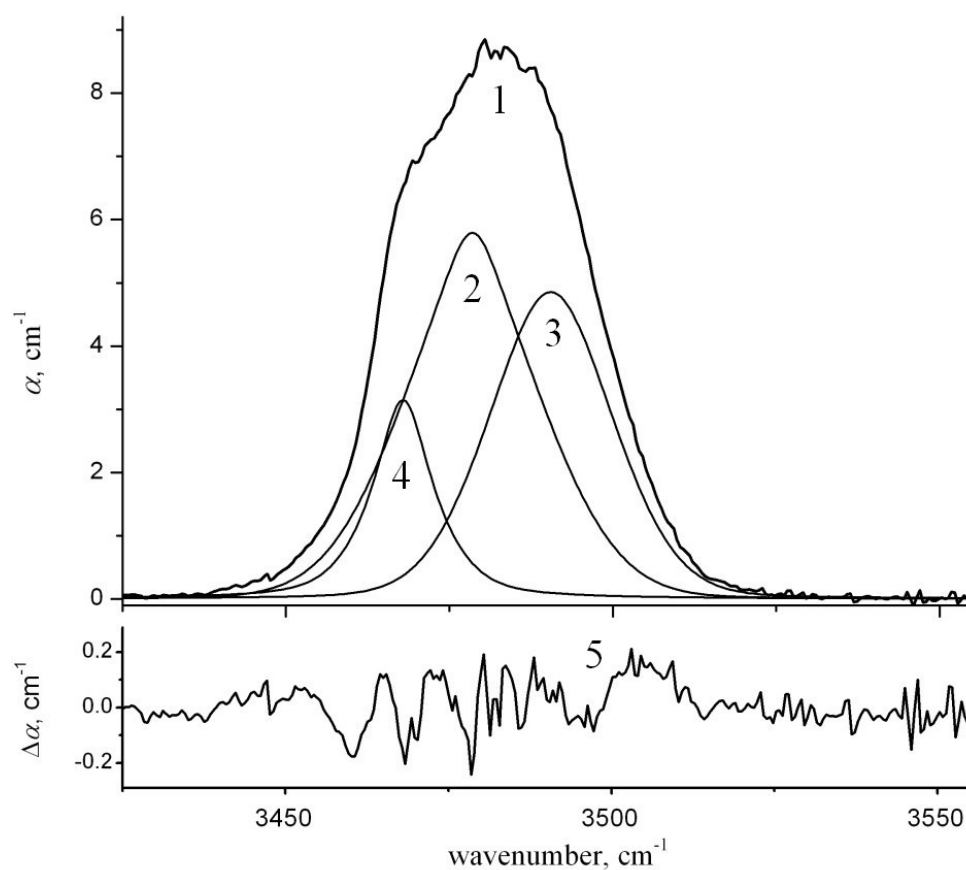
Figure 4. IR spectrum of CLN1: (1) integrated IR absorption spectrum of the CLN1 sample; (2)–(4) spectrum components; and (5) difference function $\Delta\alpha$.
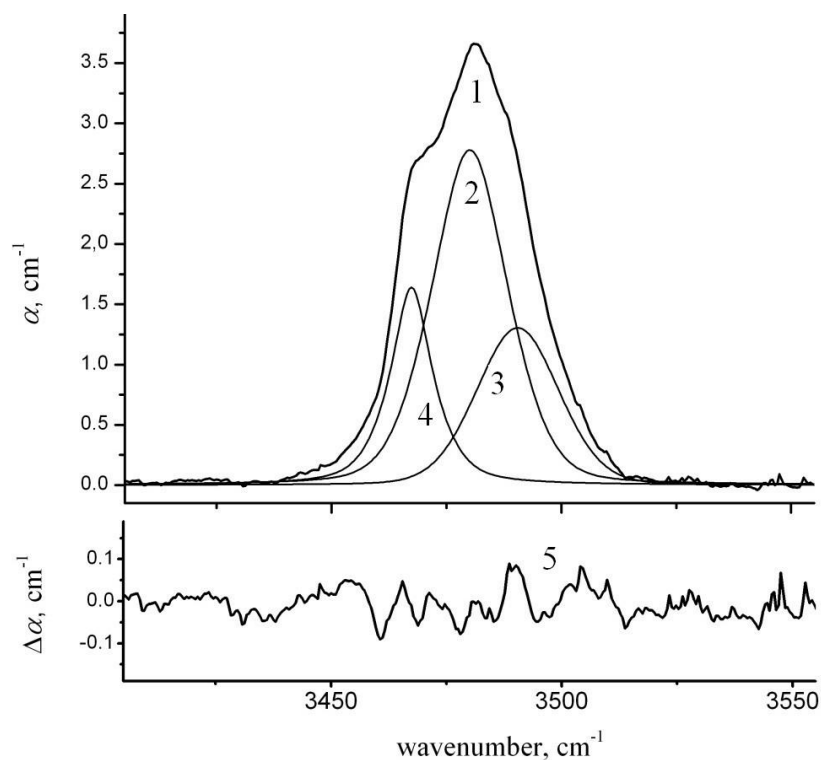

Figure 5. IR spectrum of CLN2: (1) integrated IR absorption spectrum of the CLN2 sample; (2)–(4) spectrum components; and (5) difference function $\Delta\alpha$.
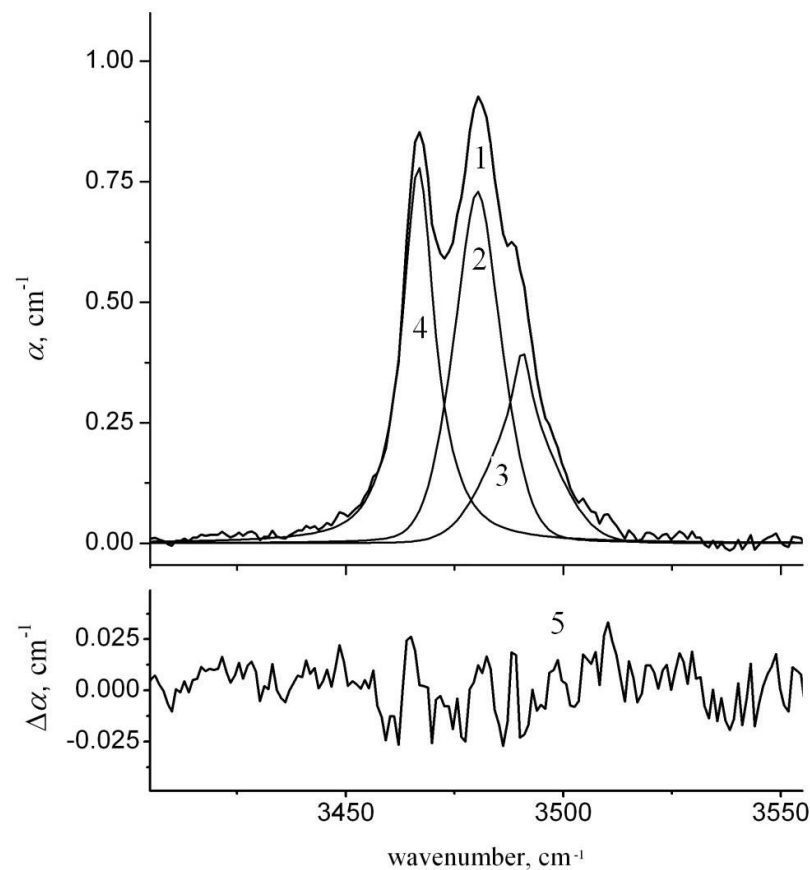
Figure 6. IR spectrum of NSLN1: (1) integrated IR absorption spectrum of the NSLN1 sample; (2)–(4) spectrum components; and (5) difference function $\Delta\alpha$.

Table 3 demonstrates the integral intensities of spectral bands obtained as a result of the decomposition of the spectrum according to options (a)–(c), as well as an estimate of the content of Li_2O in samples according to the methods [6] (column A) and [23] (column B). The volume concentration of hydrogen in CLN crystals is proportional to the integral intensity of IR absorption [29]. Data in Table 3 show that the volume concentration of hydrogen in the CLN1 sample is approximately 2.7 times higher than in CLN2.

Table 3. The IR spectra parameters of the studied LN crystals and the results of calculating R.

| Sample	I_{3466}, cm^{-2}	I_{3480}, cm^{-2}	I_{3490}, cm^{-2}	Function	μ, %	M, %	
						A	B
CLN1	60.24	132.09	118.32	G-G-G	3.1	48.86	49.31
	34.13	217.48	65.53	L-G-L	2.4	46.70	48.61
	51.72	154.81	108.46	PV-G-G	1.3	48.45	49.14
	45.99	149.44	119.03	PV-PV-PV	0.9	48.31	49.02
CLN2	34.8	58.49	31.27	L-L-L	6.2	49.13	49.56
	28.57	58.99	32.06	L-G-L	2.0	48.93	49.46
	33.36	39.64	41.7	PV-G-G	1.4	48.38	49.59
	23.94	62.60	30.67	PV-PV-PV	0.6	48.64	49.35
NSLN1	8.33	15.71	4.06	L-L-L	3.7	49.02	49.6
	8.21	9.18	7.22	L-G-L	2.6	49.42	49.66
	10.31	10.69	6.02	PV-PV-PV	1.0	49.46	49.72
NSLN2	52.94	23.65	12.66	L-G-L	4.4	49.71	49.88
	46.72	39.15	7.11	L-L-L	3.1	49.57	49.83
	47.76	32.59	8.74	PV-PV-PV	1.1	49.64	49.85
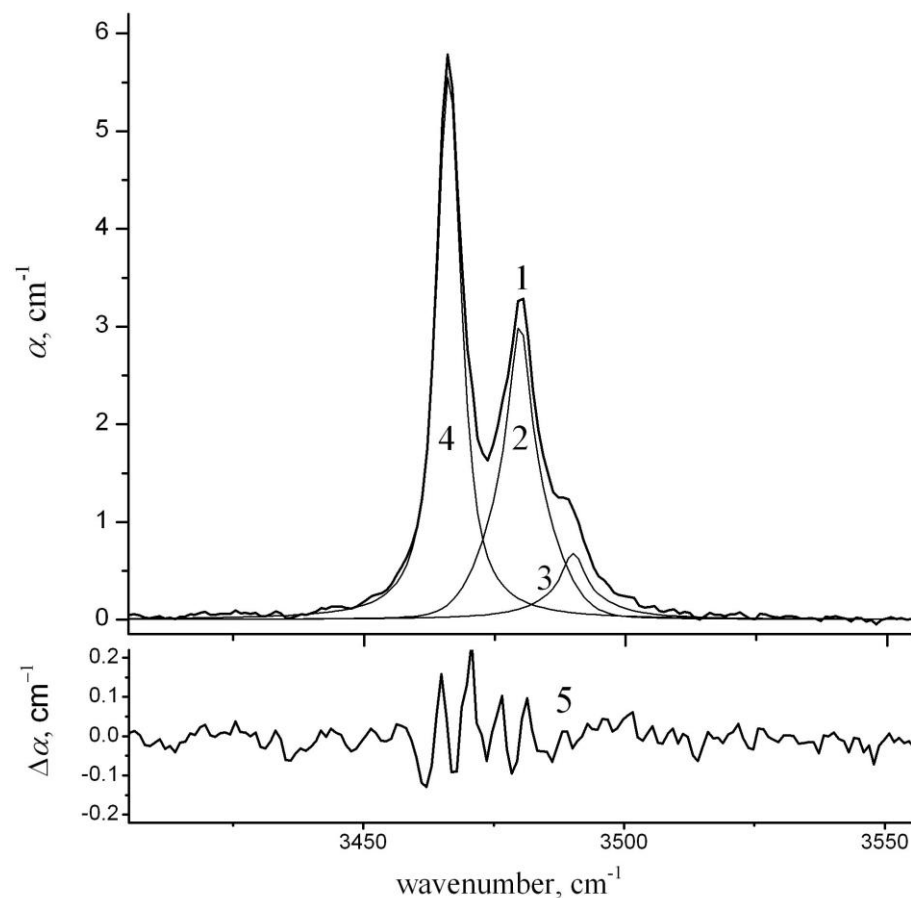
Figure 7. IR spectrum of NSLN2: (1) integrated IR absorption spectrum of the NSLN2 sample; (2)–(4) spectrum components; and (5) difference function $\Delta\alpha$.

Table 3 demonstrates that the minimal μ value for all samples including NSLN1 and NSLN2 is provided by PV distribution. The data calculated due to [6] correspond to the lowest values from Table 2.

3.2. Analysis of NMR Spectra in NSLN Samples

We determined the angular dependence of the quadrupole splitting of the ^{7}Li NMR spectrum, line width (distance between the maxima of the derivative of the absorption lines) of the central transition ($-1/2 \leftrightarrow +1/2$) $\delta\nu_0$ and two $\delta\nu_{1,2}$ quadrupole satellites, the values of the satellites second moment $(M_2)_0$, and $(M_2)_{1,2}$ at $\theta = 0°$ (θ—angle between the polar axis of the crystal Z and the direction of the external magnetic field B_o). The angular dependence of the quadrupole splitting and the value of the quadrupole coupling constant C_z for the crystals under study almost coincided with the known data for CLN and NSLN crystals [8,10].

Figure 8 presents the first derivative of the ^{7}Li NMR spectrum of the CLN3 and NSLN2 samples at $\theta = 0°$, which corresponds to the maximum splitting of spectrum lines. Both spectra contain weak side lines. Figure 8 presents their magnified versions on the left of the main spectra. The details are not seen at the main scale, so we magnified these weak side lines intensities: for CLN3 magnification is 3 times (denoted by an asterisk *3 on Figure 8), for NSLN2 − 16 times (also denoted by an asterisk *16). Weak side lines relative integral intensity N in NSLN2 is significantly smaller than that of CLN3 sample. The ^{7}Li NMR spectrum of NSLN1 is almost identical to the NSLN2 spectrum. Table 4 demonstrates the main parameters of the ^{7}Li NMR spectrum lines in the studied NSLN and CLN3 crystals for the angle $\theta = 0°$. Parameters of the ^{7}Li NMR spectrum of these crystals coincide within error with the data for a CLN crystal provided by another manufacturer [13].
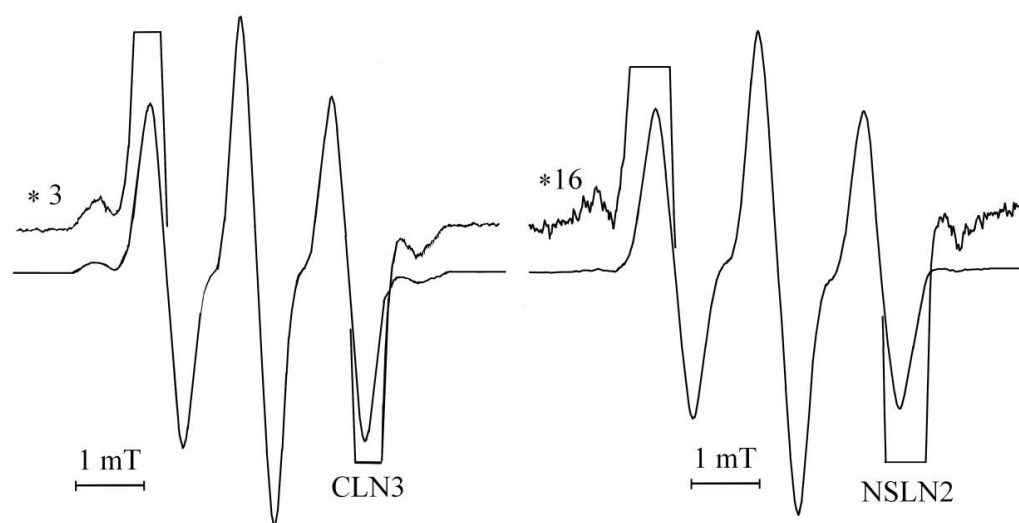
Figure 8. First derivative of ^{7}Li NMR spectrum in the CLN3 and NSLN2 samples at $\theta = 0°$. *3—the weak side lines of CLN3 magnified 3 times, *16—the weak side lines of NSLN2 magnified 16 times.

Table 4. Line parameters of the ^{7}Li NMR spectrum of three LN crystals at $\theta = 0°$.

Sample	R	$\delta\nu_0$, kHz	$\delta\nu_1$, kHz	$(M_2)_0$, kHz^2	$(M_2)_{1,2}$, kHz^2	N, %
CLN3	0.946	8.3 ± 0.2	8.8 ± 0.2	13.9 ± 0.5	19.2 ± 0.5	5 ± 1
NSLN1	~0.978	8.3 ± 0.3	8.6 ± 0.3	13.8 ± 0.7	16.0 ± 0.9	0.8 ± 0.2
NSLN2	~0.985	8.3 ± 0.3	8.5 ± 0.3	14.2 ± 0.7	15.8 ± 0.8	0.7 ± 0.2

The ^{93}Nb NMR is much more sensitive to crystal lattice defects than the ^{7}Li NMR. This is caused by a much larger quadrupole moment and the anti-screening constant of ^{93}Nb nuclei than ^{7}Li nuclei [30]. The main value of the electric field gradient (EFG) tensor V_{zz} in the Nb$_{Li}$ defect is also significantly larger than in the position of Li$_{Li}^+$ cations. Therefore, the so-called second-order quadrupole effects are more pronounced in the ^{93}Nb NMR spectra. The position of the central transition line ($-1/2 \leftrightarrow +1/2$) has a pronounced dependence on the θ angle [12,31]. Intrinsic structural defects greatly broaden both the central line of the spectrum and the quadrupole satellites [31,32].

Figure 9 demonstrates the experimentally obtained orientation dependence of the linewidth $\delta\nu(\theta)$ of the central transition of the ^{93}Nb NMR spectrum for the NSLN2 sample. The figure also presents a similar dependence for the CLN3 crystal, recorded at the same B_0 value for a comparison. Dependence $\delta\nu(\theta)$ obtained for the NSLN1 sample differs from that obtained for the NSLN2 sample by a systematic upward shift; however, it stays within the experimental errors of the same dependence of NSLN2 sample.

Note that the weak additional ^{93}Nb NMR line, which is characteristic of CLN samples [12,13], is absent from the ^{93}Nb NMR spectra of the NSLN samples. This fact confirms the assumption that its source is the core of antistite Nb$_{Li}$ defects [12,13].

3.3. Substantiation of the Applicability of Models Explaining the Complex Structure of the ^{7}Li and ^{93}Nb NMR Spectra of the LN Crystal and the Concentration Range of These Models

Previously, two models explained the appearance of additional weak lines in the ^{7}Li NMR spectrum in CLN crystals. The first of them explains the origin of these lines by the distortion of the EFG by intrinsic defects of the crystal lattice [15]. The second explains the origin by the dynamic disordering of the EFG on ^{7}Li nuclei. The disordering is attributed to the localization of Li$^+$ ions not on the 3rd order symmetry axis, but in three probable minima of the intracrystalline field potential during the rapid movement of the ion over these positions [15]. Tables 2 and 4 demonstrate that intrinsic defects hardly affect the shape of the main lines of the ^{7}Li NMR spectrum. However, integral intensity N of additional

weak sidelines is approximately proportional to the relative amount of Nb_{Li} antisite ions N′. The unambiguous relationship between the value of N and the number of antisite defects testifies in favor of the first model, i.e., the defective attribution of these lines. Note that exactly the same conclusion was made on the basis of the computer simulation of the ^{7}Li NMR spectra in the $LiTaO_3$ crystal, which is isostructural to LN [33].
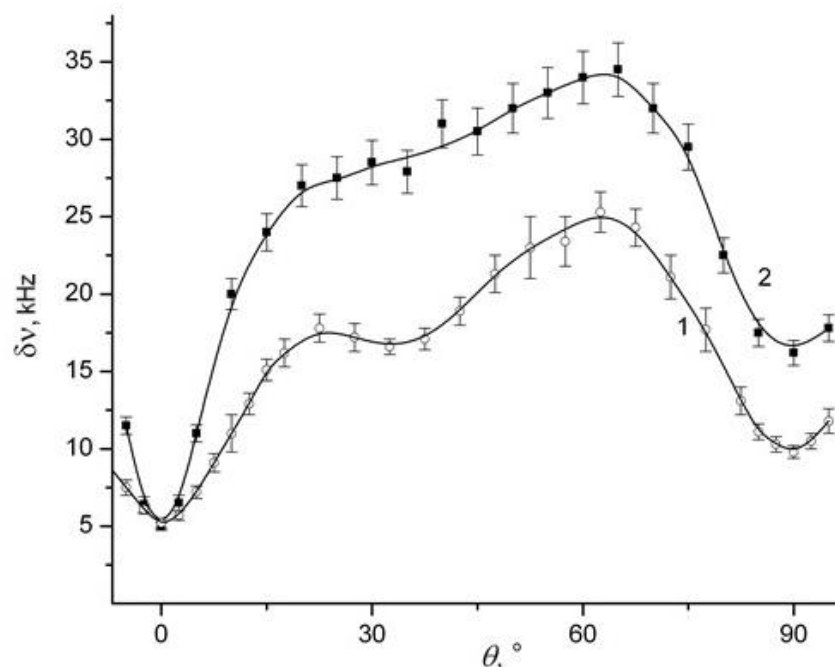

Figure 9. Angular dependence of the line width of the central transition of the [93]Nb NMR spectrum in samples (1) NSLN2 and (2) CLN3.

Figure 9 clearly demonstrates that the line of the central transition of the [93]Nb NMR spectrum of both NSLN and CLN3 samples in most crystal orientations in a magnetic field is much wider than in an ideal crystal lattice. In an ideal lattice the width of the NMR lines is determined only by magnetic dipole—dipole interactions and for LN crystals these values are: $\delta\nu_{d-d} \sim 4.2$ kHz at $\theta = 0°$ and $\delta\nu_{d-d} \sim 4.5$ kHz at $\theta = 90°$. Thus, the obtained results differ both qualitatively and quantitatively from those presented in [11].

We carried out computer simulation of the angular dependence $\delta\nu(\theta)$ for LN samples with different deviations from stoichiometry for the value $B_o = 1.4$ T. The simulation takes into account the set of random realizations of the EFG on [93]Nb nuclei, caused by the number of ($Nb_{Li} + 4V_{Li}$) defect complexes corresponding to the deviation from stoichiometry [34,35]. The influence of local distortions of the structure was taken into account by introducing an additional misorientation of the EFG tensor main axis Z on [93]Nb nuclei relative to the c axis of the crystal and a spread in the values of the main component of the EFG V_{zz}. The calculation algorithm is the same as before [14,33]. The parameters were chosen from the condition of optimal correspondence between the simulated and experimental results. Figure 10 demonstrates the results of modeling $\delta\nu(\theta)$.

Figure 10 clearly demonstrates that simulation results and experimental data for the CLN3 and NSLN samples agree quite satisfactorily. This indicates the correctness of the approach used. Even at $[Li_2O] = 49.9$ mol%, the width of the NMR lines remains much larger than the value determined by magnetic dipole—dipole interactions. [93]Nb NMR can be used to analyze the stoichiometry and defectiveness of NSLN crystals.
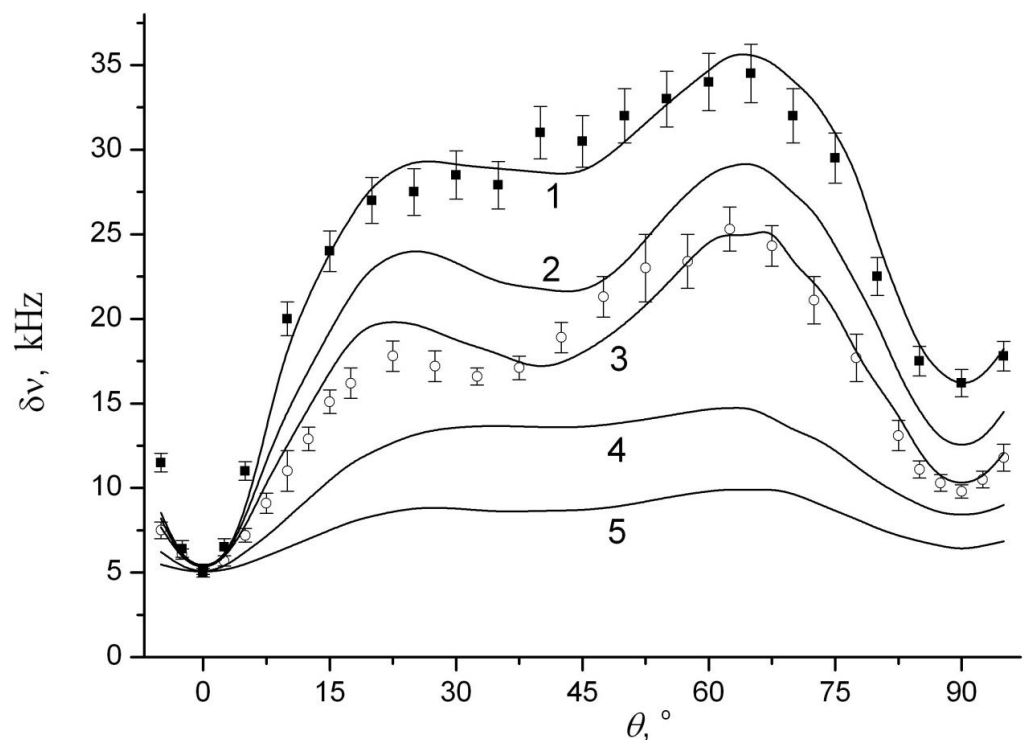
Figure 10. The results of modeling the angular dependence of the ^{93}Nb NMR linewidth for: (1) M = 48.4 mol%; (2) M = 49.2 mol%; (3) M = 49.6 mol%; (4) M = 49.8 mol%; and (5) M = 49.9 mol%.

4. Conclusions

Analysis of the IR spectra of the NSLN and CLN samples showed that the approach proposed in [6] is applicable for a much wider range of R values than its authors had assumed. A strong systematic overestimation of the obtained values was observed when the second well-known method for calculating R [23] was used.

The methods of mathematical processing of the contours of the lines of the IR spectrum of crystals were evaluated, and methods were chosen that most accurately determine the stoichiometry of LN crystals of various compositions.

Even small deviations from stoichiometry in nominally pure LN crystals strongly affected the shape of the NMR line of the central transition of the ^{93}Nb NMR spectrum. The line broadened inhomogeneously over almost the entire range of crystal orientations in a magnetic field. The latter confirmed the possibility and extended the range of applicability of the NMR method for the analysis of the defect structure of NSLN crystals at least up to [Li$_2$O] = 49.9 mol%. Thus, IR spectroscopy and ^{93}Nb NMR are probably the most sensitive and complementary methods to the presence of intrinsic defects in LN crystals.

Author Contributions: Conceptualization, M.P., N.S. and A.Y.; methodology, A.Y.; validation, S.Y.; investigation, A.Y. and S.Y.; writing—original draft preparation, A.Y., M.P. and N.S.; writing—review and editing, M.P.; visualization, A.Y. and S.Y.; supervision, M.P. and A.Y. All authors have read and agreed to the published version of the manuscript.

Institutional Review Board Statement: Not applicable.

Informed Consent Statement: Not applicable.

Data Availability Statement: The raw data supporting this study are available from a corresponding author, M.P., on a reasonable request.

Conflicts of Interest: The authors declare no conflict of interest.

References

1. Volk, T.R.; Wöhlecke, M. *Lithium Niobate. Defects, Photorefraction and Ferroelectric Switching*; Springer: Berlin, Germany, 2008.
2. Abrahams, S.C. *Properties of Lithium Niobate*; INSPEC, The Institution of Engineering and Technology: New York, NY, USA, 1989; 234p.
3. Gunter, P.; Huignard, J.P. *Photorefractive Materials and Their Applications. Part 1*; Springer: Berlin, Germany, 2006; 243p.
4. Prokhorov, A.M.; Kuzminov, Y.S. *Physics and Chemistry of Crystalline Lithium Niobate*; Adam Hilger: New York, NY, USA, 1990; 237p.
5. Lines, M.E.; Glass, A.M. *Principles and Application of Ferroelectrics and Related Materials*; Clarendon Press: Oxford, UK, 1977; p. 680.
6. Lengyel, K.; Péter, A.; Kovács, L.; Corradi, G.; Pálfalvi, L.; Hebling, J.; Unferdorben, M.; Dravecz, G.; Hajdara, I.; Szaller, Z.; et al. Growth, defect structure, and THz application of stoichiometric lithium niobate. *Appl. Phys. Rev.* **2015**, *2*, 040601. [CrossRef]
7. Slichter, C.P. *Principles of Magnetic Resonance*, 3rd ed.; Springer: Berlin/Heidelberg, Germany; New York, NY, USA, 1996.
8. Peterson, G.E.; Carruthers, J.R. ^{93}Nb NMR as a sensitive and accurate probe of stoichiometry in LiNbO$_3$ crystals. *J. Solid St. Chem.* **1969**, *1*, 98–99. [CrossRef]
9. Peterson, G.E.; Carruthers, J.R.; Carnevale, A. ^{93}Nb NMR study of the LiNbO$_3$–LiTaO$_3$ solid-solution system. *J. Chem. Phys.* **1970**, *53*, 2436–2442. [CrossRef]
10. Charnaya, E.V.; Gabrielyan, V.T.; Kasperovich, V.S.; Klimko, S. Li^7 NMR in LiNbO$_3$ crystals with different nonstoichiometry. *Ferroelectrics* **1997**, *202*, 115–119. [CrossRef]
11. Malovichko, G.; Grachev, V.; Schirmer, O. Interrelation of intrinsic and extrinsic defects—Congruent, stoichiometric, and regularly ordered lithium niobate. *Appl. Phys. B* **1999**, *68*, 785–793. [CrossRef]
12. Peterson, G.E.; Carnevale, A. ^{93}Nb NMR linewidths in nonstoichiometric lithium niobate. *J. Chem. Phys.* **1972**, *56*, 4848–4851. [CrossRef]
13. Yatsenko, A.V.; Ivanova-Maksimova, H.M.; Sergeev, N.A. NMR study of intrinsic defects in congruent LiNbO$_3$. *2. Overlapping defects. Phys. B* **1998**, *254*, 256–259. [CrossRef]
14. Yatsenko, A.V.; Yevdokimov, S.V.; Sugak, D.Y.; Solskii, I.M. Investigation of the defect complexes in highly Mg-doped LiNbO$_3$ crystals by ^{93}Nb NMR method. *Func. Mater.* **2014**, *21*, 31–35. [CrossRef]
15. Yatsenko, A.V.; Ivanova, E.N.; Sergeev, N.A. NMR study of intrinsic defects in congruent LiNbO$_3$. *1. Unoverlapping defects. Phys. B* **1998**, *240*, 254–262. [CrossRef]
16. Palatnikov, M.N.; Sidorov, N.V.; Kadetova, A.V.; Teplyakova, N.A.; Makarova, O.V.; Manukovskaya, D.V. Concentration threshold in optically nonlinear LiNbO$_3$:Tb crystals. *Opt. Las. Technol.* **2021**, *137*, 106821. [CrossRef]
17. Palatnikov, M.N.; Kadetova, A.V.; Aleshina, L.A.; Sidorova, O.V.; Sidorov, N.V.; Biryukova, I.V.; Makarova, O.V. Growth, structure, physical and chemical characteristics in a series of LiNbO$_3$:Er crystals of different composition grown in one technological cycle. *Opt. Las. Techol.* **2022**, *147*, 107671. [CrossRef]
18. Fedorova, E.P.; Aleshina, L.A.; Sidorov, N.V.; Chufyrev, P.G.; Yanichev, A.A.; Palatnikov, M.N.; Voskresenskii, V.M.; Kalinnikov, V.T. Stoichiometry and doping effects on cation ordering in LiNbO$_3$ crystals. *Inorg. Mater.* **2010**, *46*, 206–211. [CrossRef]
19. Serrano, M.D.; Bermudez, V.; Arizmendi, L.; Dieguez, E. Determination of the Li/Nb ratio in LiNbO$_3$ crystals grown by Czochralski method with K$_2$O added to the melt. *J. Cryst. Growth* **2000**, *210*, 670. [CrossRef]
20. Polgar, K.; Peter, A.; Foldvari, I. Crystal growth and stoichiometry of LiNbO$_3$ prepared by the flux method. *Opt. Mater.* **2002**, *19*, 7. [CrossRef]
21. Yatsenko, A.V.; Yevdokimov, S.V. A nuclear magnetic resonance probe for testing substances with large values of T$_1$. *Instrum. Exp. Tech.* **2003**, *46*, 57–59. [CrossRef]
22. Kovács, L.; Shalay, V.; Capelletti, R. Stoichiometry dependence of the OH- absorption band in LiNbO$_3$ crystals. *Sol. St. Comm.* **1984**, *52*, 1029–1984. [CrossRef]
23. Chen, H.; Shi, L.; Yan, W.; Chen, G.; Shen, J.; Li, Y. OH$^-$ absorption bands of LiNbO$_3$ with varying composition. *Chin. Phys. B* **2009**, *18*, 2372. [CrossRef]
24. Sidorov, N.V.; Smirnov, M.V.; Teplyakova, N.A.; Palatnikov, M.N. Photoluminescence and particular features of the defect structure of congruent and near-stoichiometric lithium niobate crystals obtained using different technologies. *Opt. Spectrosc.* **2020**, *128*, 635–641. [CrossRef]
25. Bäumer, C.; David, C.; Betzler, K.; Hesse, H.; Lengyel, K.; Kovács, L.; Wöhlecke, M. Composition dependence of the OH-stretch-mode spectrum in lithium tantalate. *Phys. Stat. Sol. A* **2004**, *201*, R13–R16. [CrossRef]
26. Salloum, M.Y.; Grunsky, O.S.; Man'shina, A.A.; Tver'yanovich, A.S.; Tver'yanovich, Y.S. Investigation of lithium niobate composition by optical spectroscopy methods. *Russ. Chem. Bull.* **2009**, *58*, 2228–2232. [CrossRef]
27. Kovács, L.; Wöhlecke, M.; Jovanović, A.; Polgar, K.; Kapphan, S. Infrared absorption study of the OH$^-$ vibrational band in LiNbO$_3$ crystals. *J. Phys. Chem. Sol.* **1991**, *52*, 797–803. [CrossRef]
28. Köhler, T.; Mehner, E.; Hanzig, J.; Gärtner, G.; Stöcker, H.; Leisegang, T.; Meyer, D.C. Real structure influencing the hydrogen defect chemistry in congruent LiNbO$_3$ and LiTaO$_3$. *J. Sol. St. Chem.* **2016**, *244*, 108–115. [CrossRef]
29. Klauer, S.; Wöhlecke, M.; Kapphan, S. Influence of H-D isotopic substitution on the protonic conductivity of LiNbO$_3$. *Phys. Rev. B* **1992**, *45*, 2786–2799. [CrossRef]

30. Hennel, J.W.; Klinowski, J. *Fundamentals of Nuclear Magnetic Resonance*; Longman Scientific & Technical: Essex, UK; John Wiley & Sons: New York, NY, USA, 1993; p. 288.
31. Kind, R.; Gränicher, H.; Derighetti, B.; Waldner, F.; Brun, E. NMR of ^{93}Nb in ferroelectric LiNbO$_3$. *Sol. St. Comm.* **1968**, *6*, 439–440. [CrossRef]
32. Peterson, G.E.; Bridenbaugh, P.M. NMR study of ferroelectric LiNbO$_3$ and LiTaO$_3$. *II. J. Chem. Phys.* **1968**, *48*, 3402–3406. [CrossRef]
33. Yatsenko, A.V.; Palatnikov, M.N.; Sidorov, N.V. Investigation of the intrinsic defects of LiTaO$_3$ crystals by NMR spectroscopy. *Cryst. Rep.* **2019**, *64*, 36–40. [CrossRef]
34. Kim, S.; Gopalan, V.; Kitamura, K.; Furukawa, Y. Domain reversal and nonstoichiometry in lithium tantalate. *J. Appl. Phys.* **2001**, *90*, 2949. [CrossRef]
35. Gopalan, V.; Dierolf, V.; Scrymgeour, D. Defect–domain wall interactions in trigonal ferroelectrics. *Annu. Rev. Mater. Res.* **2007**, *37*, 449. [CrossRef]